


Parameter independent low-power heteronuclear decoupling for fast magic-angle spinning solid-state NMR

Journal Article

Author(s):

Eqbal, Asif; Madhu, Perunthiruthy K.; Meier, Beat H.; Nielsen, Niels C.; [Ernst, Matthias](#) ; Agarwal, Vipin

Publication date:

2017-02-28

Permanent link:

<https://doi.org/10.3929/ethz-b-000129417>

Rights / license:

[In Copyright - Non-Commercial Use Permitted](#)

Originally published in:

The Journal of Chemical Physics 146(8), <https://doi.org/10.1063/1.4976997>

Parameter independent low-power heteronuclear decoupling for fast magic-angle spinning solid-state NMR

Asif Equbal,^{1,2} P. K. Madhu,^{1,3} Beat H. Meier,⁴ Niels Chr. Nielsen,^{2, a)} Matthias Ernst,^{4, b)} and Vipin Agarwal^{1, c)}

¹⁾ *TIFR Centre for Interdisciplinary Sciences, 21 Brundavan Colony, Narsingi, Hyderabad 500 075, India*

²⁾ *Center for Insoluble Protein Structures (inSpin) and Center for Ultrahigh-Field NMR Spectroscopy, Interdisciplinary Nanoscience Center (iNANO) and Department of Chemistry, Aarhus University, Gustav Wieds Vej 14, DK-8000 Aarhus C, Denmark*

³⁾ *Department of Chemical Sciences, Tata Institute of Fundamental Research, Homi Bhabha Road, Colaba, Mumbai 400005, India*

⁴⁾ *Physical Chemistry, ETH Zurich, Vladimir-Prelog-Weg 2, 8093 Zurich, Switzerland*

(Dated: 2017/02/01)

Abstract

Major advances have recently been made in the field of heteronuclear dipolar decoupling in solid-state NMR. These developments have improved the resolution and sensitivity of the NMR spectrum of spins coupled to protons. One such new scheme, denoted as rCW^{ApA} , has proven to be robust with practically no need for parameter optimization (*Chemical Physics Letters*, 583, 2013, 1). Most of the experiments with rCW^{ApA} have been carried out in the regimes of slow to moderate magic-angle spinning while simultaneously applying high decoupling radio-frequency amplitudes. Here, we explore the performance of the rCW^{ApA} sequence and its predecessor rCW^A in the regime of low-power radio-frequency irradiation and fast magic-angle spinning. The robustness of the refocused continuous-wave (rCW) schemes to experimental parameters such as pulse lengths and offset irradiation is demonstrated. Numerical simulations and analytical theory have been used to understand the effects of various nuclear spin interactions on the decoupling performance of the low-power rCW decoupling scheme relative to other decoupling methods. This has led to the design of an ‘*optimum low-power decoupling sequence*’ that can be used without parameter optimization. This result is particularly important in the context of samples with low signal to noise.

a)ncn@au.dk

b)maer@ethz.ch

c)vipina@tifrh.res.in

INTRODUCTION

Efficient heteronuclear decoupling in rotating solids is vital for obtaining high-resolution NMR spectra of low- γ nuclear spins such as ^{13}C and ^{15}N . Heteronuclear decoupling in the solid state is challenging primarily due to the large magnitude of the couplings and multi-spin effects that manifest in the form of higher-order cross terms between different anisotropic nuclear spin interactions.¹⁻²⁶ A further important consideration for spin decoupling in magic-angle-spinning (MAS) experiments is to minimize the interference between the spatial (due to MAS) and spin (due to RF pulse) rotations.^{22,25,27-29} This is typically achieved by setting the RF field amplitude (ν_1) several times higher than the MAS frequency, ν_r , (*i.e.*, $\nu_1 > 4\nu_r$) or lower (*i.e.*, $\nu_r > 4\nu_1$).^{1,17}

For slow to intermediate MAS frequencies, $\nu_r < 35$ kHz, RF-field amplitudes in the range of 80-120 kHz often provide reasonable decoupling performance. For higher MAS frequencies, it becomes increasingly impractical to irradiate, especially sensitive biological samples, with high-amplitude RF pulses as they may cause deleterious sample heating. In addition, such high RF-field amplitudes set strong demands on the hardware. For fast spinning ($\nu_r > 45$ kHz), low-power decoupling approach is preferred with $\nu_1 < \nu_r/4$.^{1,17} This approach is particularly attractive for spectroscopy, as the combination of fast MAS and low-power RF irradiation typically allows faster repetition of experiments and is less demanding on the electronics of the probe and the sample.

In terms of the number of experimental parameters to be optimized, heteronuclear decoupling methods can be broadly classified into three groups (assuming ν_1 is known): a) *Two or more parameters optimization*: Sequences such as two-pulse phase modulation (TPPM),⁷ SPINAL¹⁰ and their variants^{11,14-16} typically require optimization of at least two parameters (pulse lengths and one or two phases). At slow to intermediate spinning frequencies, these schemes are currently the most commonly used ones, especially in case of biological molecules, despite the fact that optimization is often impossible on such samples. b) *One parameter optimization*: The X-inverse-X (XiX)¹² family of schemes has an advantage over the TPPM family of schemes as XiX scheme requires only one parameter (pulse length) optimization. In the low-power fast-MAS regime, two new schemes have been proposed, namely, AM-XiX and Sc-AM-XiX (Fig. 1).¹⁹ They show improved decoupling efficiency compared to the original XiX sequence. The new schemes are basically only amplitude-modulated

(AM-XiX) and combined amplitude- and phase-modulated (Sc-AM-XiX) version of XiX. The amplitude modulation and super-cycling modifications help to improve decoupling efficiency of the original XiX sequence. c) *No optimization*: Symmetry-based sequences⁴ and continuous-wave (CW)⁵ irradiations are the only decoupling sequences where in principle no optimization is required. However, the latter methods are typically avoided either due to lower decoupling efficiency in case of CW or very high RF amplitude requirement in case of symmetry-based schemes.

The recently introduced alternative decoupling approach, denoted as refocused continuous-wave (*r*CW) decoupling, invokes a novel concept of interleaving CW irradiation with short refocusing π pulses.^{23,24} Like XiX, this scheme also has only one optimizable parameter. An extensive experimental and theoretical comparison of the XiX and *r*CW^A schemes showed that both these schemes are quite similar in their decoupling conditions and mechanism in the high-power regime.³⁰ Both these sequences are impeded primarily by higher-order cross terms between heteronuclear and homonuclear dipolar couplings.³⁰ The basic *r*CW^A decoupling scheme has been improved with the recently proposed phase-alternated variant, *r*CW^{ApA}.²⁵ This scheme has shown higher decoupling efficiency while simultaneously offering robustness towards mismatch in experimental parameters like pulse lengths and RF amplitudes at different MAS frequencies, practically making it optimization independent and in turn ensuring a much simpler set-up of near optimum decoupling condition in the high RF-power regime *i.e.*, the $\nu_1 > 4\nu_r$ case.

So far *r*CW schemes have mainly been used in the regime of high RF-amplitude decoupling where the refocusing π pulse is treated in the limit of delta pulses.²³ This condition cannot be met in the low RF-amplitude regime where a π pulse can typically be few times longer than the rotor period. In this study, we demonstrate that the *r*CW decoupling schemes can also be used for low-power decoupling, by tweaking the scheme with respect to the refocusing pulse and hence circumventing the necessity for a high-power π pulse. Here, two *r*CW schemes are considered, the basic one, *r*CW^A (Fig. 1a), and its phase-alternated version, *r*CW^{ApA} (Fig. 1b). The objective of this article is to introduce a low-power heteronuclear decoupling method which is very efficient, robust and most importantly eliminates the need for any parameter optimization. This is a prerequisite for decoupling sequences to be useful in biomolecular solid-state NMR spectroscopy where extensive parameter optimization is impractical.

FIG. 1: Schematics of heteronuclear dipolar decoupling pulse sequences: (a) rCW^A , (b) rCW^{ApA} , (c) XiX, (d) AM-XiX, and (e) Sc-AM-XiX.

II. NUMERICAL SIMULATIONS

Using numerical simulations, we first analyze the decoupling performance of the two rCW schemes with respect to the two experimental parameters: $\beta_x = \omega_1 \tau_x$ and $\beta_y = \omega_1 \tau_y$, with τ_x and τ_y denoting the duration of the β_x and β_y pulses, respectively. The decoupling efficiency is monitored using the normalized peak height obtained after Fourier transformation of the free-induction-decay (FID).

Fig. 2 shows the normalized peak height as a function of the β_x and β_y flip angles for the ^{13}C resonance of a $^{13}\text{CH}_2$ spin system simulated for rCW^A (Fig. 2a) and rCW^{ApA} (Fig. 2b) decoupling at a MAS frequency $\nu_r = 58.8235$ kHz and an RF-field amplitude $\nu_1 = 10$ kHz. For numerical convenience, ν_r is set to this number. In the case of rCW^A , significant loss in intensity is observed when the flip angle β_x is close to odd multiples of 90° or when β_y is close to odd multiples of 180° . A number of additional weak resonance conditions are also observed (marked with black dotted lines) which will be referred to as "slanting resonance conditions". These resonance conditions depend on the modulation frequency ($\omega_m = \frac{1}{\tau_c}$ where $\tau_c = 2 * \tau_x + \tau_y$ for rCW^A and $\tau_c = 4 * \tau_x + 2 * \tau_y$ for rCW^{ApA}) of the sequence and the spinning frequency of the sample and are more pronounced at shorter cycle times (τ_c). In the case of rCW^{ApA} , where β_y is around an integer multiple of 360° , a significant loss in intensity is observed except when β_x is an integer multiple of 180° . These conditions correspond to the low-power XiX decoupling conditions where the flip angle has to be an integer multiple of 360° . The slanting resonance conditions observed for rCW^A are also observed for the rCW^{ApA} scheme.

In general, ^1H CSA and ^1H - ^1H dipolar-coupling interactions manifest themselves indirectly via cross terms with the heteronuclear dipolar interaction and induce residual terms which may have detrimental effects on the decoupling performance of any sequence. The

effect of these anisotropic interactions can be independently evaluated through numerical simulations. To this end, we alternatively remove the ^1H CSA and ^1H - ^1H dipolar coupling interactions in a $^{13}\text{CH}_2$ spin system and observe the decoupling performance as a function of the parameters β_x and β_y (Figs. 2c-f).

Fig. 2c-d show the normalized intensity of the ^{13}C resonance as a function of β_x and β_y for $r\text{CW}^A$ and $r\text{CW}^{ApA}$ when the ^1H - ^1H dipolar interactions are set to zero. All other parameters are the same as those in Figs. 2a-b. In the case of $r\text{CW}^A$, without the ^1H - ^1H dipolar-coupling interactions (Fig. 2c), all the prominent resonance conditions at β_x close to odd integer multiples of 90° and at β_y close to odd integer multiples of 180° (Fig. 2a) vanish indicating that the cross term between the homonuclear-heteronuclear dipolar-coupling interaction is the cause for the loss in intensity at these conditions. For $r\text{CW}^{ApA}$ (Fig. 2d), the same terms are responsible for the loss in intensity observed at $\beta_y = n360^\circ$ in Fig. 2b. In the absence of ^1H - ^1H dipolar-coupling interactions, only the slanting resonances are observed, which appear to become weaker as the cycle time of the pulse scheme increases.

Fig. 2e-f show plots where the ^1H CSA interaction are set to zero while all the other interactions are present. Comparing Figs. 2a, c, and e, the deleterious resonance conditions appearing at β_y equal to integer multiples of 360° (when $\beta_x > 180^\circ$) appear on account of cross terms between CSA and heteronuclear dipolar interaction. Such resonance conditions are stronger in Fig. 2c where the homonuclear dipolar interactions are absent. For $r\text{CW}^{ApA}$ (Fig. 2f), removal of CSA leads to increase in the decoupling efficiency for higher values of β_y compared to the case in Fig. 2d. It may be inferred that for a fixed β_x , the effect of ^1H CSA increases as β_y increases.

Simulations of the two low-power $r\text{CW}$ decoupling sequences show that the region where both the homonuclear and the CSA cross terms become small is very narrow in the case of $r\text{CW}^A$ while in the case of $r\text{CW}^{ApA}$ the two cross terms are simultaneously minimized over a broader span of pulse parameters, for $\beta_y < 180^\circ$ and $\beta_x \approx 360^\circ$.

III. THEORY

In this section we validate the numerical findings theoretically. In order to decipher the role of different interactions for the low-power $r\text{CW}$ decoupling schemes, we follow the generalized theoretical approach to understand heteronuclear decoupling by Tan et al.²¹

FIG. 2: Numerically simulated peak height observed for the ^{13}C resonance of a $^{13}\text{CH}_2$ spin system using $r\text{CW}^A$ (a, c, e) and $r\text{CW}^{ApA}$ (b, d, f) decoupling sequences as a function of their parameters β_x and β_y . The simulations were done with all interactions present (a, b), with ^1H - ^1H dipolar-coupling interaction turned off (c,d) and the ^1H CSA interaction turned off (e,f). The simulations closely mimicked experimental conditions at a 700 MHz NMR instrument with $\nu_{\text{r}} = 58.8235$ kHz and $\nu_1 = 10$ kHz. Dotted lines mark the resonance conditions. The flip angles were varied in steps of 3.6° .

The rotating-frame Hilbert-space spin Hamiltonian for a spin S (observable, *e.g.* ^{13}C or ^{15}N) coupled to N I spins (*e.g.* ^1H) during decoupling is,

$$H(t) = \sum_{n=-2}^2 \left[\sum_{j=1}^N \omega_j^{(n)} I_{jz} + \omega_{Sj}^{(n)} I_{jz} S_z + \sum_{i<j} \omega_{ij}^{(n)} (3I_{iz} I_{jz} - I_i \cdot I_j) \right] e^{in\omega_{\text{r}}t} + \omega_1(t) \sum_{j=1}^N (I_{jx} \cos(\phi(t)) + I_{jy} \sin(\phi(t))) \quad (1)$$

where $\omega_j^{(n)}$, $\omega_{Sj}^{(n)}$, and $\omega_{ij}^{(n)}$ are the n^{th} order Fourier coefficients of the I_j spin CSA, $I_j S$ heteronuclear dipolar coupling, and $I_i I_j$ homonuclear dipolar-coupling tensors, respectively. The internal Hamiltonian is transformed into the interaction frame of the decoupling pulse sequence using the unitary operator, $U_{\text{rf}}(t) = T e^{-i \int_0^t H_{\text{rf}}(t') dt'}$ (T being the Dyson time ordering operator³¹) as

$$\tilde{H}(t) = U_{\text{rf}}^{-1}(t) H(t) U_{\text{rf}}(t) \quad (2)$$

Here, basically the I_z operator gets modulated in the interaction frame as,

$$\tilde{I}_z(t) = \sum_{\chi=x,y,z} a_{\chi}(t) I_{\chi} \quad (3)$$

The Hamiltonian in the RF interaction frame has multiple time dependencies. A general treatment of a multiple time-dependent Hamiltonian is achieved by Floquet theory^{32,33} which requires that the Hamiltonian is periodic in time. In general, the interaction-frame Hamiltonian is not necessarily cyclic with respect to the modulation frequency ($\omega_{\text{m}} = 2\pi/\tau_{\text{c}}$) of a

sequence. However, using an additional, effective field ($\omega_{\text{eff}} = \beta_{\text{eff}}/\tau_c$), it becomes possible to write any RF interaction-frame Hamiltonian as a periodic function.³⁴ The effective frequency, ω_{eff} , in this work has been calculated using Quaternions.^{35,36} Quaternion is a mathematical formalism typically applied to study mechanics in 3D space. They can also be used to define rotations in 3D space. In case of rCW^A scheme:

$$\beta_{\text{eff}} = 2\cos^{-1}[(\cos(\beta_x/2)\cos(\beta_y/2) - \sin(\beta_x/2)\sin(\beta_y/2)\cos(\beta_z/2)] \quad (4)$$

In case of rCW^{ApA} , β_{eff} is simply equal to $2\beta_y$. Notably, in the rCW^{ApA} case, ω_{eff} is zero when β_y equals an integer multiple of π . In the interaction frame, we can write

$$\tilde{I}_z(t) = \sum_{\chi=x,y,z} \sum_{k,\ell} a_{\chi}^{k,\ell} e^{ik\omega_m t} e^{i\ell\omega_{\text{eff}} t} I_{\chi} \quad (5)$$

Therefore, the general form of the interaction-frame Hamiltonian can be written as

$$\tilde{H}(t) = \sum_{n=-2}^2 \sum_{k=-\infty}^{\infty} \sum_{\ell=-2}^2 \tilde{H}^{(n,k,\ell)} e^{in\omega_r t} e^{ik\omega_m t} e^{i\ell\omega_{\text{eff}} t} \quad (6)$$

All the $a_{\chi}^{k,\ell}$ coefficients obey the conjugation relation $(a_{\chi}^{k,\ell})^* = a_{\chi}^{-k,-\ell}$, which is necessary to ensure that the total interaction-frame Hamiltonian remains Hermitian. To the first order, the interaction-frame Hamiltonian $\tilde{H}(t)$ is averaged to zero (neglecting the isotropic J couplings) provided none of the following resonance conditions are satisfied:

$$n_0\omega_r + k_0\omega_m + \ell_0\omega_{\text{eff}} = 0 \quad (7)$$

At the resonance conditions, the heteronuclear dipolar-coupling Hamiltonian can get recoupled and cause broadening of the S -spin signal. For these first-order resonance conditions, n_0 can only be ± 1 or ± 2 whereas k_0 can be any integer and ℓ_0 can only take values of ± 1 or 0 . The width of resonance condition depends on the magnitude of the $a_{\chi}^{k,\ell}$ coefficients corresponding to the $I_{\chi}S_z$ operators in the H_{IS} component of the Hamiltonian ($\chi=x, y, z$). For zero effective field ω_{eff} , the resonance condition will simplify to $n\omega_r + k\omega_m = 0$ or $\omega_r/\omega_m = k/n$, *i.e.* ω_r/ω_m equalling an integer or half-integer number. For non-zero values of ω_{eff} , additional resonances are observed which are shifted from the bimodal conditions, to an extent depending on the magnitude of ω_{eff} . The resonant dipolar Hamiltonian has contributions from the higher orders of the effective Hamiltonian also and should be avoided in order to obtain efficient spin decoupling. We will highlight the dominant deleterious second-order resonance conditions, after discussing the second-order Hamiltonian, calculated with van Vleck perturbation theory^{29,34,37-42}, which in general is of the form

FIG. 3: The magnitude of the second-order residual dipolar-coupling scaling factors, $\log_{10}(\sum_x q_X^{IS\otimes I})$ (a, b, c, d) and $\log_{10}(\sum_{\mu,\chi} q_{\gamma\chi}^{IS\otimes II})$ (e, f, g, h) for the $|\nu| = 1$ (a, c, e, g) and $|\nu| = 2$ (b, d, f, h) Fourier indices calculated using van-Vleck perturbation theory for rCW^A (a, b, e, f) and rCW^{ApA} (c, d, g, h) decoupling schemes. $\log_{10}(\sum_x q_X^{IS\otimes I})$ is the scaling factor for chemical-shift induced residual coupling and $\log_{10}(\sum_{\mu,\chi} q_{\gamma\chi}^{IS\otimes II})$ is the scaling factor for homonuclear induced dipolar coupling. The white spaces in g) and h) denotes $\log_{10}(\sum_{\mu,\chi} q_{\gamma\chi}^{IS\otimes II})$ to be smaller than < -12 for rCW^{ApA} .

$$\tilde{H}_{(2)}^{(n_0, k_0, \ell_0)} = -\frac{1}{2} \sum_{\nu, \kappa, \lambda} \frac{[\tilde{H}^{(n_0 - \nu, k_0 - \kappa, \ell_0 - \lambda)}, \tilde{H}^{(\nu, \kappa, \lambda)}]}{\nu\omega_r + \kappa\omega_m + \lambda\omega_{\text{eff}}} \quad (8)$$

Here $\tilde{H}_{(2)}^{(n_0, k_0, \ell_0)}$ terms with all n_0 , k_0 , and ℓ_0 equalling zero constitute the non-resonant part of the Hamiltonian. These are always present and determine the residual line width under decoupling. $\tilde{H}_{(2)}^{(n_0, k_0, \ell_0)}$ with non-zero n_0 , k_0 , and ℓ_0 are called resonant terms as their contribution becomes important only at specific (resonance) conditions. Since the non-resonant parts determine the residual line width, we will discuss their behaviour for the two sequences.

A. Effective Hamiltonian

In the second-order effective Hamiltonian, the residual coupling Hamiltonian is predominantly influenced by the presence of two types of cross terms, $\tilde{H}_{(IS\otimes I)}^{(0,0,0)}$ and $\tilde{H}_{(IS\otimes II)}^{(0,0,0)}$, given by:

$$\tilde{H}_{\text{eff}}^{IS} = \tilde{H}_{(IS\otimes I)}^{(0,0,0)} + \tilde{H}_{(IS\otimes II)}^{(0,0,0)} \quad (9)$$

These two terms are represented as²¹:

$$\tilde{H}_{(IS\otimes I)}^{(0,0,0)} = \sum_j \sum_{\nu=-2}^2 \sum_{\chi=x,y,z} i q_{\chi}^{\nu} (\omega_j^{(\nu)} \omega_{S_j}^{(-\nu)} + \omega_j^{(-\nu)} \omega_{S_j}^{(\nu)}) S_z I_{j\chi} \quad (10)$$

$$\tilde{H}_{(IS\otimes II)}^{(0,0,0)} = \sum_{j \neq l} \sum_{\nu=-2}^2 \sum_{\gamma,\chi=x,y,z} -i 3 (q_{\gamma\chi}^{\nu} \omega_{jl}^{(\nu)} \omega_{S_j}^{(-\nu)} + (q_{\gamma\chi}^{\nu})^* \omega_{jl}^{(-\nu)} \omega_{S_j}^{(\nu)}) S_z I_{j\gamma} I_{l\chi} \quad (11)$$

and will be referred to as CSA cross term and dipolar-coupling cross term, respectively. The CSA and dipolar-coupling cross terms are proportional to the scaling factors, $q_X^{IS\otimes I} = \sum_{\kappa} \sum_{\lambda} \frac{\epsilon_{\delta\mu\chi} a_{\delta}^{-\kappa,-\lambda} a_{\mu}^{\kappa,\lambda}}{\nu\omega_r + \kappa\omega_m + \lambda\omega_{\text{eff}}}$ and $q_{\gamma\chi}^{IS\otimes II} = \sum_{\kappa} \sum_{\lambda} \frac{\epsilon_{\delta\mu\chi} a_{\delta}^{-\kappa,-\lambda} a_{\mu}^{\kappa,\lambda}}{\nu\omega_r + \kappa\omega_m + \lambda\omega_{\text{eff}}}$, where $\epsilon_{\delta\mu\chi}$ is the Levi-Civita symbol. Fig. 3 maps the magnitude of both the scaling factors, $\sum_{\chi} q_X^{IS\otimes I}$ and $\sum_{\gamma,\chi} q_{\gamma\chi}^{IS\otimes II}$ in \log scale for the spatial components $|\nu|=1$ (Figs. 3a, c, e, g) and $|\nu|=2$ (Figs. 3b, d, f, h) as a function of pulse flip angles for rCW^A (Figs. 3a, b, e, f) and rCW^{ApA} (Figs. 3c, d, g, h) decoupling schemes. The larger the values of $\log_{10}(q)$ the less efficient decoupling. The Fourier coefficients of the two spin operators, $a_{\mu\gamma}^{\kappa,\lambda}$, are calculated as described previously²¹.

For rCW^A (Figs. 3 a, b) the magnitude of $q^{IS\otimes I}$ is maximum when either β_x or β_y is close to zero. This condition would basically mimic CW decoupling which is strongly affected by the CSA cross term. The CSA cross term would be minimal for the region mapped in blue color. In the case of rCW^{ApA} (Figs. 3 c, d), the magnitude of $q^{IS\otimes I}$ tends to increase with increasing β_y . The cross terms are minimal for β_y close to zero. This represents the XiX decoupling sequence where it is known that the CSA cross terms are eliminated. For a fixed τ_y , $q^{IS\otimes I}$ decreases in strength as the β_x flip angle increases thereby leading to better decoupling as seen in the simulations also. The homonuclear dipolar-coupling induced terms for the rCW^A scheme depend on the parameters β_x and β_y unlike in the case of the rCW^{ApA} scheme where it is negligible for all the conditions except for β_y equaling integer multiples of 360° , which are the XiX conditions. The $q^{IS\otimes II}$ scaling factors are minimal in case of rCW^A only when either β_x is multiples of 180° , or β_y is multiples of 360° . It is worth noting that the pulse parameters where the CSA cross terms are minimal are not the same as where the dipolar cross terms are minimal, implying that the CSA and the homonuclear dipolar effects cannot be simultaneously minimized in the rCW^A scheme. Here we consider the contribution of only the second-order cross terms for the relevant interactions. In order to understand the poor performance of the decoupling sequence in certain regions, it is also necessary to explicitly consider the different orders of interactions especially close to the resonance conditions.

FIG. 4: A map of $\Delta=(\omega_m - 2\omega_{\text{eff}})$ resonance conditions for (a) rCW^A and (b) rCW^{ApA} schemes. The resonance condition gets satisfied when Δ is close to zero.

Apart from the non-resonant part of the effective Hamiltonian, the resonant terms can also introduce residual dipolar interactions which are of the form $\tilde{H}^{(n_0, k_0, \ell_0)}$ or $\tilde{H}_{(2)}^{(n_0, k_0, \ell_0)}$ with $n_0\omega_r + k_0\omega_m + \ell_0\omega_{\text{eff}}=0$, as discussed earlier. The second-order resonance conditions are similar to the first-order resonance conditions except that n_0 can also take values of 0, ± 3 , and ± 4 and ℓ_0 can additionally take values of ± 2 . In particular, the resonances corresponding to $n=0$ would be the strongest as the associated scaling factors for such conditions will be the largest in magnitude. The $n_0=0$ condition will lead to the resonance: $k_0\omega_m + \ell_0\omega_{\text{eff}} = 0$. A map of $\Delta=(\omega_m - 2\omega_{\text{eff}})$ resonance condition is shown in Fig. 4 for the rCW^A and rCW^{ApA} schemes. The resonance condition gets satisfied when Δ becomes zero (Fig. 4). Such resonances are important mainly in the rCW^A scheme (Fig. 4a). It can be clearly seen that $q^{IS\otimes I}$ is larger when the β_y flip angle corresponds to 360° . Similar kinds of resonance conditions also recouple $IS \otimes II$ cross terms. The magnitude of $q^{IS\otimes II}$ becomes dominant when the β_y flip angle is an odd multiple of 180° and the β_x flip angle is an odd multiple of 90° . For the rCW^{ApA} scheme, the dipolar recoupling corresponding to the $n_0 = 0$ conditions are negligibly small in the second-order Hamiltonian (Fig. 4b). The only relevant resonance conditions for the rCW^{ApA} decoupling are when τ_c/τ_r equals an odd integer. Such decoupling conditions must be avoided for optimum decoupling performance. The theoretical findings here match well with the numerical simulations in the previous section.

IV. RESULTS AND DISCUSSIONS

The findings from the numerical simulations and the Floquet analysis are substantiated by experimental analysis shown in Fig. 5. The features of only the rCW^{ApA} scheme are analysed here as it is more robust and efficient than rCW^A with respect to the experimental parameters. Fig. 5a maps normalized peak height of the $^{13}\text{C}_\alpha$ resonance of $1,2\text{-}^{13}\text{C},^{15}\text{N}$ -

glycine ethyl ester obtained with rCW^{ApA} decoupling as a function of β_x and β_y under the conditions, $\nu_r = 60$ kHz and $\nu_1 = 10$ kHz, on a 700 MHz spectrometer. The experimentally observed resonance conditions are similar to those observed in the analytical and numerical simulation (Figs. 2b, 3e and 3f). For $\beta_y = 0^\circ$ and 360° , good decoupling conditions are obtained only when $\beta_x = 180^\circ$ and 360° . At these conditions, rCW^{ApA} reduces to the low-power XiX decoupling condition where the best decoupling corresponds to a flip angle of 360° .³⁹ The slanting resonances are also observed experimentally at the conditions similar to those observed in the simulations, *i.e.* when the condition $n_0\omega_r + k_0\omega_m + l_0\omega_{\text{eff}} = 0$ is satisfied. However, in the simulations, these resonance conditions are narrow and sharp while in experiments they are smeared out, which might be due to multi-spin effects or RF inhomogeneity. For a fixed τ_y , the effective cycle frequency of the decoupling block decreases as τ_x increases. At small values of ω_{eff} , the resonance conditions can be approximated to the bimodal conditions: $n_0\omega_r + k_0\omega_m = 0$. *i.e.* $\tau_c/\tau_r = n/k$. Plotting the parameter map as a function of τ_c/τ_r and β_y shows these resonance conditions more clearly (Fig. 5b). The resonance conditions are observed when τ_c becomes an odd integer multiple of τ_r . At the same time, the good decoupling conditions are observed at $\tau_c = N\tau_r$ where N is an even integer. N should be chosen such that τ_c should be approximately $4 \times 360^\circ$ or in other words N should be an even integer close to the ratio $4\nu_r/\nu_1$. This condition implies that the length of each of the CW block and half the τ_y pulse should correspond to a 360° rotation. For example, when $\nu_r = 60$ kHz and $\nu_1 = 10$ kHz, the $4\nu_r/\nu_1$ ratio is 24, ensuring that good decoupling can be obtained by fixing τ_c/τ_r to 22, 24, or 26. Empirically, we observe that good decoupling is observed when $2\tau_y$ is between $0.1\tau_c$ to $0.3\tau_c$ while independently ensuring that τ_y does not correspond to a 360° flip angle pulse (Fig. 5c). A simple arithmetic calculation shows that $\tau_y = 0.075N\tau_r$ and $\tau_x = 0.2125N\tau_r$ for optimum decoupling. The dependence of the decoupling efficiency on the τ_y pulse is illustrated in Fig. 5c, where the decoupling efficiency is monitored by varying τ_y for fixed $\tau_c = 20, 22, \text{ or } 24 \tau_r$. This implies that in the $\nu_1 < \nu_r/4$ decoupling regime, decoupling parameters τ_y and τ_x are related to ν_r and are therefore free of any optimization. Beside ν_r , the only other parameter required for efficient decoupling is the approximate knowledge of ν_1 . The rotor-linked optimum decoupling parameter observed in Fig. 5 has been confirmed for different experimental conditions. This is illustrated further in the supplementary material. The τ_y parameter behaves differently in the low-power and high-power decoupling regimes. In the high-power decoupling regime, the length of the y -

FIG. 5: Normalized, experimental peak heights observed for the $^{13}\text{C}_\alpha$ resonance of 1,2- ^{13}C , ^{15}N -glycine ethyl ester using $r\text{CW}^{ApA}$ decoupling. The experiments were recorded with $\nu_r = 60$ kHz and $\nu_1 = 10$ kHz. (a) peak heights plotted as a function of β_x and β_y . The flip angles were varied in steps of 5.4° . (b) The peak heights replotted as a function of τ_c/τ_r and β_y . (c) Normalized peak height as a function of parameter τ_y/τ_c for different ratios of τ_c/τ_r

FIG. 6: (a) shows the $^{13}\text{C}_\alpha$ peak of 1,2- ^{13}C , ^{15}N -glycine ethyl ester obtained with various decoupling schemes at a) $\nu_r = 60$ kHz and $\nu_1 = 10$ kHz recorded on a 700 MHz NMR instrument and (b) similar to (a) with $\nu_r = 50$ kHz.

pulse should strictly correspond to a 180° pulse²⁵ while in the low-power regime the y -pulse can take a wide range of values. This happens because the cycle time, τ_c , is the more critical parameter in case of low-power decoupling.

We now compare the decoupling efficiency of the $r\text{CW}$ schemes with the low-power XiX family of decoupling schemes. Fig. 6a compares the performance of different decoupling sequences under conditions of fast spinning ($\nu_r = 60$ kHz) and low RF amplitude ($\nu_1 = 10$ kHz) for $^{13}\text{C}_\alpha$ peak of 1,2- ^{13}C , ^{15}N -glycine ethyl ester. The comparison shows that $r\text{CW}^{ApA}$ performs slightly better than the other schemes. The performance of $r\text{CW}^A$, AM-XiX, and Sc-AM-XiX is comparable, within a range of 5-10% while XiX performance is substantially worse. At $\nu_r = 50$ kHz, similar trend in decoupling efficiency is observed (Fig. 6b). Local parameter optimization was required to obtain efficient decoupling conditions for all the schemes except, $r\text{CW}^{ApA}$. These spectra were obtained at on-resonance proton irradiation conditions. The optimum decoupling conditions for each decoupling scheme is summarized in Table 1.

In the low-power RF irradiation regime, the decoupling efficiency is strongly dependent

TABLE I: Optimum decoupling conditions at low-RF amplitude and fast MAS frequency

	General conditions	$\nu_r=60$ kHz, $\nu_1=10$ kHz
rCW^A	$\tau_c/\tau_r \approx 2\nu_r/\nu_1^*$, $\beta_y \approx 270^\circ$	$\tau_c/\tau_r = 12$, $\beta_y = 259^\circ$
rCW^{ApA}	$\tau_c/\tau_r \approx 4\nu_r/\nu_1^\dagger$, $2\tau_y/\tau_c \approx 0.15$	$\tau_c/\tau_r = 24$, $2\tau_y/\tau_c = 0.15$
XiX	$\tau_p \approx 360^\circ$ or 720°	$\tau_p = 350^\circ$
AM-XiX	$\tau_p/\tau_r \approx \nu_r/\nu_1^\ddagger$, $\nu_{cw} \approx 0.5\nu_m$	$\tau_p/\tau_r = 6$, $\nu_{cw} = 2.5$ kHz
Sc-AM-XiX	$\tau_p/\tau_r \approx \nu_r/\nu_1^\ddagger$, $\nu_{cw} \approx 1 - 3$ kHz	$\tau_p/\tau_r = 6$, $\nu_{cw} = 2.25$ kHz

Note: * An integer; \dagger An even integer; \ddagger A half integer or multiples.

FIG. 7: Normalized experimental peak heights observed for the $^{13}C_\alpha$ resonance of 1,2- $^{13}C,^{15}N$ -glycine ethyl ester showing (a) offset dependence and (b) transverse dephasing profile for various decoupling schemes, recorded with $\nu_r = 60$ kHz and $\nu_1 = 10$ kHz.

on the carrier-frequency offset. Previous reports indicate a drop in peak intensity of 40-60 % at small offsets of about 4-5 ppm.^{20,21} Here we analyze the offset dependence of rCW^{ApA} scheme for different values of τ_c . In Fig. 7a, we compare the offset dependence of the various decoupling sequences by varying the offset (ppm) in carrier frequency and fixing the pulse parameters at the optimum condition for each of the sequences. Clearly, rCW^{ApA} and Sc-AM-XiX seem to be more robust to offset effects than other sequences.

We also measured the T'_2 value for various decoupling using a spin-echo pulse scheme at $\nu_1 = 10$ kHz and $\nu_r = 60$ kHz. The intensity/magnetisation decay curve for various sequences is shown in Fig. 7b. rCW^{ApA} , rCW^A , and AM-XiX scheme have similar and longer T'_2 value as compared to Sc-AM-XiX, XiX and CW decoupling. Under off-resonance conditions, schemes like rCW^{ApA} and Sc-AM-XiX would be superior as they are in general more tolerant towards RF offset.

METHODS: EXPERIMENTS AND SIMULATIONS

The experiments were carried out on a Bruker Avance III wide-bore 700 MHz NMR spectrometer (Bruker Biospin, Rheinstetten, Germany) using a commercial Bruker 1.3 mm ^1H - ^2H - ^{13}C - ^{15}N four-channel MAS and a 1.3 mm ^1H -X two-channel MAS probe. U- ^{13}C , ^{15}N -glycine (Sigma-Aldrich) and U- ^{13}C , ^{15}N -glycine ethyl ester (produced as a derivative from U- ^{13}C , ^{15}N -glycine) were used for the experiments. Ramped-amplitude cross polarization (CP)⁴³ was used to achieve ^1H to ^{13}C polarization transfer. Heteronuclear decoupling pulses were applied during the detection of the ^{13}C FID. Peak heights obtained after Fourier transformation of the FID were used for quantitative comparisons. In all the experiments, the recycle delays were set to 2 s and 4 scans were accumulated.

Numerical and analytical simulations were performed using the open-source simulation software package, SIMPSON^{44,45} and GAMMA⁴⁶, respectively. Simulations were performed for a typical aliphatic CH_2 spin system using the following parameters⁴⁷ (assuming operation on a 700 MHz NMR spectrometer): ^1H CSA and asymmetry, $\delta_{\text{H}}^{\text{CSA}} = -2450$ Hz and $\eta_{\text{H}}^{\text{CSA}} = 0$, ^{13}C CSA and asymmetry $\delta_{\text{C}}^{\text{CSA}} = 0$ Hz, $\eta_{\text{C}}^{\text{CSA}} = 0$ with isotropic shifts of $\delta_{\text{H}1}^{\text{iso}} = 0$ Hz, $\delta_{\text{H}2}^{\text{iso}} = 200$ Hz, $\delta_{\text{C}}^{\text{iso}} = 0$ Hz, J -couplings $\omega_{\text{HC}}^{\text{J}}/2\pi = 130$ Hz (for both C-H pairs), heteronuclear dipolar couplings of $\omega_{\text{HC}}^{\text{D}}/2\pi = -23.3$ kHz (for both protons) and homonuclear dipolar coupling of $\omega_{\text{HH}}^{\text{D}}/2\pi = -21.3$ kHz. Powder averaging was achieved using REPULSION⁴⁸ with 20 $\{\alpha_{\text{CR}}, \beta_{\text{CR}}\}$ crystallite orientations and 10 γ_{CR} angles. The decoupling efficiency of the two $r\text{CW}$ sequences was compared by calculating the evolution of the ^{13}C resonance (on-resonance) while applying the decoupling pulses on the ^1H spins and monitoring peak height obtained after Fourier transformation of the FID.

VI. CONCLUSIONS

In this paper, we have analyzed the performance of different variants of the $r\text{CW}$ decoupling in the low-power and fast MAS regime. The results demonstrate that for $r\text{CW}^{\text{ApA}}$, the knowledge of MAS frequency and RF field is sufficient to accurately predict efficient decoupling conditions. No further optimization of experimental parameters τ_x and τ_y is required. The following guidelines must be observed for setting up good decoupling: a) for a given ν_r and ν_1 , calculate the ratio $4 * \nu_r/\nu_1$ and round it off to the nearest even integer,

b) set $\tau_c(4 * \tau_x + 2 * \tau_y) = N * \tau_r$ and c) ensure, $\tau_y = 0.075\tau_c$ and $\tau_x = 0.2125\tau_c$. For example, if $\nu_r = 60$ kHz and $\nu_1 = 13$ kHz then $4\nu_r/\nu_1 = 18.46$. For this case $\tau_c = (16$ or 18 or $20) * \tau_r$ would provide the optimum decoupling. A simple calculation gives $\tau_y = 0.075N\tau_r = 22.5 \mu s$ and $\tau_x = 0.2125N\tau_r = 63.7 \mu s$ for $N=18$. In addition, rCW^{ApA} provides longer T'_2 values and is tolerant towards RF-offset. The low-power rCW^{ApA} conditions discussed here should be valid for MAS frequencies above 45 kHz. Initial results in our laboratory indicate a superior decoupling performance of low-power rCW^{ApA} even at 111 kHz MAS frequency. These aspects make rCW^{ApA} particularly attractive for use on samples with low-signal to noise under fast MAS.

SUPPLEMENTARY MATERIAL

See supplementary material for numerically simulated and experimental plots of intensity as a function of experimental parameter β_x and β_y for different combinations of proton decoupling field and MAS frequencies. A Bruker cpd program has also been included for implementation on a Bruker spectrometer.

ACKNOWLEDGEMENTS

We acknowledge the National Facility for High Field NMR, TIFR, Mumbai and TCIS Hyderabad. The project was supported by grants from the Danish National Research Foundation (DNRF59) and the European Commission under the Seventh Framework Programme (FP7), contract Bio-NMR 261863 and from the Swiss National Science Foundation (SNF grants 200020_146757 and 200020_159797). We thank Mr. Manoj Naik and Dr. Morten Bjerring for technical assistance.

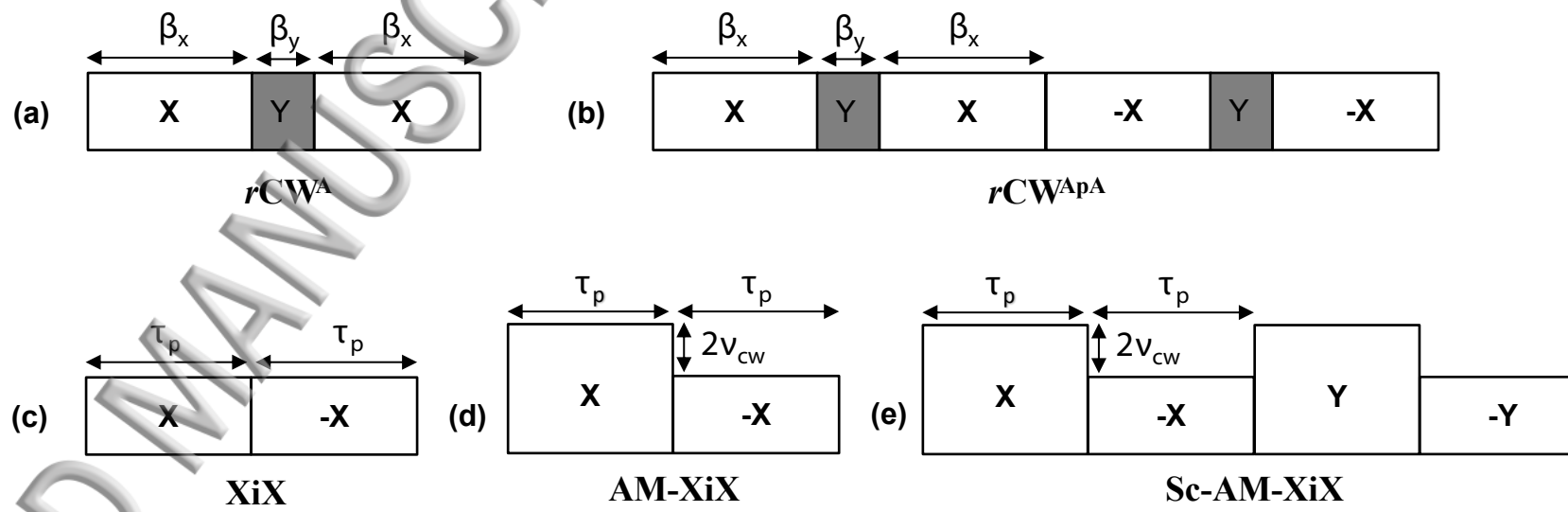
REFERENCES

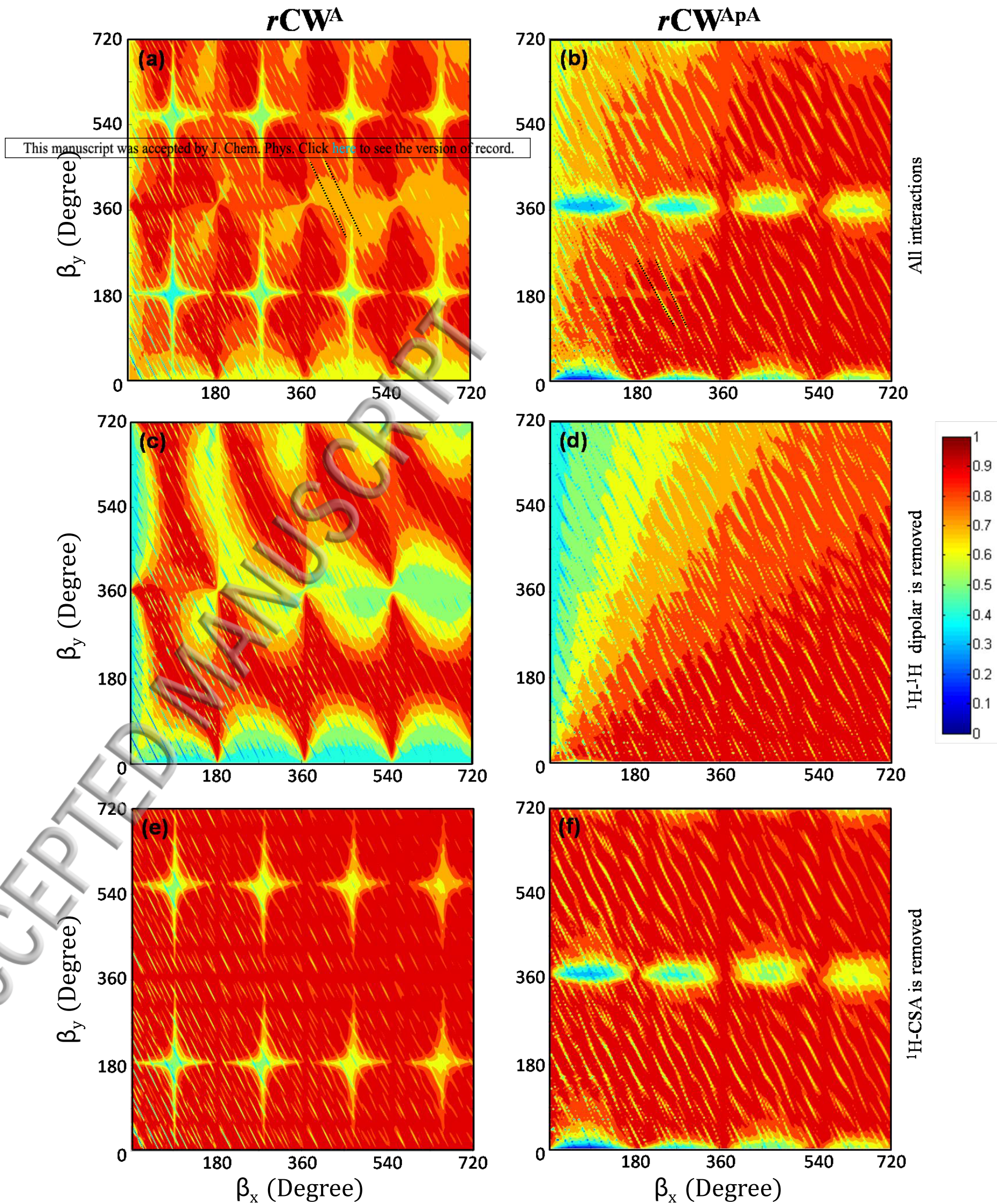
- ¹M. Ernst, Heteronuclear spin decoupling in solid-state NMR under magic-angle sample spinning, *J. Magn. Reson.* 162 (2003) 1.
- ²P. Hodgkinson, Heteronuclear decoupling in the NMR of solids, *Prog. Nucl. Magn. Reson. Spectrosc.* 46 (2005) 159.
- ³P.K. Madhu, Heteronuclear spin decoupling in solid-state nuclear magnetic resonance: Overview and outlook, *Isr. J. of Chem.* 54 (2014) 25.
- ⁴M. H. Levitt, Symmetry-based pulse sequences in magic-angle spinning solid-state NMR, in: D. M. Grant, R. K. Harris (Eds.), *Encyc. of NMR*, John Wiley & Sons, Chichester (2002).
- ⁵A.L. Bloom, J.N. Shoolery, Effects of perturbing radiofrequency fields on nuclear spin coupling, *Phys. Rev.* 97 (1955) 1261.
- ⁶P. Tekely, P. Palmas, D. Canet, Effect of proton spin exchange on the residual ¹³C MAS NMR linewidths. Phase-modulated irradiation for efficient heteronuclear decoupling in rapidly rotating solids, *J. Magn. Reson.* A107 (1994) 129.
- ⁷A.E. Bennett, C.M. Rienstra, M. Auger, K.V. Lakshmi, R.G. Griffin, Heteronuclear decoupling in rotating solids, *J. Chem. Phys.* 103 (1995) 6951.
- ⁸Z.H. Gan, R.R. Ernst, Frequency- and phase-modulated heteronuclear decoupling in rotating solids, *Solid State Nucl. Magn. Reson.* 8 (1997) 153.
- ⁹M. Edén, M.H. Levitt, Pulse sequence symmetries in the nuclear magnetic resonance of spinning solids: application to heteronuclear decoupling, *J. Chem. Phys.* 111 (1999) 1511.
- ¹⁰B.M. Fung, A.K. Khitrin, K. Ermolaev, An improved broadband decoupling sequence for liquid crystals and solids, *J. Magn. Reson.* 142 (2000) 97.
- ¹¹K. Takegoshi, J. Mizokami, T. Terao, ¹H decoupling with third averaging in solid NMR, *Chem. Phys. Lett.* 341 (2001) 540.
- ¹²A. Detken, E.H. Hardy, M. Ernst, B.H. Meier, Simple and efficient decoupling in magic-angle spinning solid-state NMR, *Chem. Phys. Lett.* 56 (2002) 298.
- ¹³G. D. Paëpe, D. Sakellariou, P. Hodgkinson, S. Hediger, L. Emsley, Heteronuclear decoupling in NMR of liquid crystals using continuous phase modulation, *Chem. Phys. Lett.* 368 (2003) 511.

- ¹⁴R. S. Thakur, N.D. Kurur, P.K. Madhu, Swept-frequency two-pulse phase modulation for heteronuclear dipolar decoupling in solid-state NMR, Chem. Phys. Lett. 426 (2006) 459.
- ¹⁵V.S. Mithu, P.K. Madhu, Exploring connections between phase-modulated heteronuclear dipolar decoupling schemes in solid-state NMR, Chem. Phys. Lett. 556 (2013) 325.
- ¹⁶A. Equbal, S. Paul, V.S. Mithu, P.K. Madhu, N.C. Nielsen, *r*TPPM: Towards improving solid-state NMR two-pulse phase-modulation heteronuclear dipolar decoupling sequence by refocusing, J. Magn. Reson. 244 (2014) 68.
- ¹⁷M. Ernst, A. Samoson, B. Meier, Low-power decoupling in fast magic-angle spinning NMR, Chem. Phys. Lett. 348 (2001) 293.
- ¹⁸M. Ernst, A. Samoson, B. Meier, Low-power XiX decoupling in NMR, J. Magn. Reson. 163 (2003) 332-339.
- ¹⁹V. Agarwal, T. Tuherm, A. Reinhold, J. Past, A. Samoson, M. Ernst, B. H. Meier, Amplitude-modulated low-power decoupling sequences for fast magic-angle spinning NMR, Chem. Phys. Lett. 583 (2013) 1.
- ²⁰V.S. Mithu, S. Paul, N.D. Kurur, P.K. Madhu, Heteronuclear dipolar decoupling in solid-state nuclear magnetic resonance under ultra-high magic-angle spinning, J. Magn. Reson. 209 (2011) 359.
- ²¹K. O. Tan, V. Agarwal, B. H. Meier, M. Ernst, A generalized theoretical framework for the description of spin decoupling in solid-state MAS NMR: Offset effect on decoupling performance, J. Chem. Phys. 145 (2016) 094201.
- ²²M. Weingarth, P. Tekely, G. Bodenhausen, Efficient heteronuclear decoupling by quenching rotary resonance in solid-state NMR, Chem. Phys. Lett. 466 (2008) 247.
- ²³J.M. Vinther, A.B. Nielsen, M. Bjerring, E.R.H. van Eck, A.P.M. Kentgens, N. Khaneja, N.C. Nielsen, Refocused continuous-wave decoupling: A new approach to heteronuclear dipolar decoupling in solid-state NMR spectroscopy, J. Chem. Phys. 137 (2012) 214202.
- ²⁴A. Equbal, S. Paul, V.S. Mithu, P.K. Madhu, N.C. Nielsen, Efficient heteronuclear decoupling in MAS solid-state NMR using non-rotor-synchronized *r*CW irradiation, J. Magn. Reson. 246 (2014) 104.
- ²⁵A. Equbal, M. Bjerring, P.K. Madhu, N.C. Nielsen, Improving spectral resolution in biological solid-state NMR using phase-alternated *r*CW heteronuclear decoupling, Chem. Phys. Lett. 635 (2015) 339.

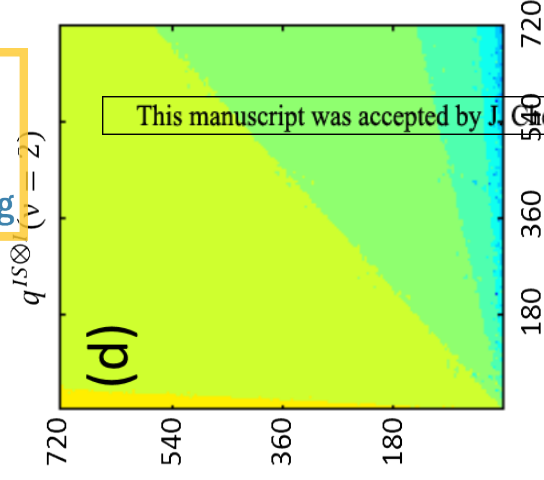
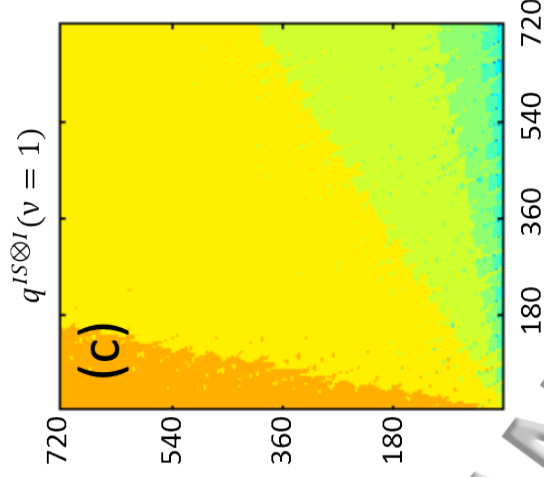
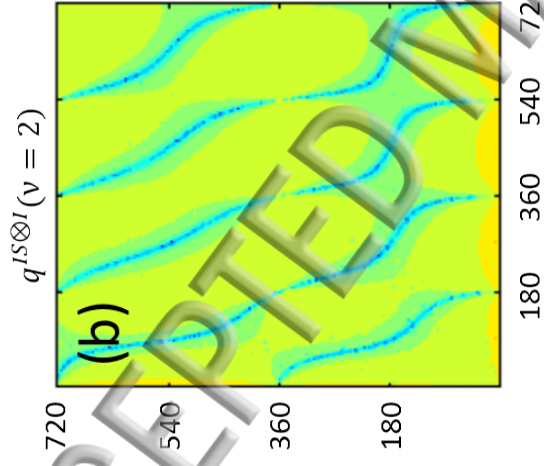
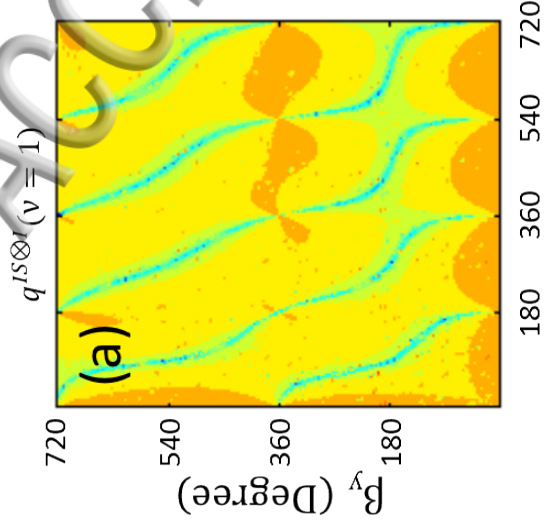
- ²⁶A. Equbal, M. Bjerring, P.K. Madhu, N.C. Nielsen, A unified heteronuclear decoupling strategy for magic-angle-spinning solid-state NMR spectroscopy, *J. Chem. Phys.* 142 (2015) 184201.
- ²⁷A. Equbal, M. Bjerring, K. Sharma, P.K. Madhu, N.C. Nielsen, Heteronuclear decoupling in MAS NMR in the intermediate to fast sample spinning regime, *Chem. Phys. Lett.* 644 (2016) 243.
- ²⁸K. Sharma, P.K. Madhu, V. Agarwal, Systematic evaluation of heteronuclear spin decoupling in solid-state NMR at the rotary-resonance conditions in the regime of fast magic-angle spinning, *J. Magn. Reson.* 270 (2016) 136.
- ²⁹M. Ernst, A. Samoson, B.H. Meier, Decoupling and recoupling using continuous-wave irradiation in magic-angle-spinning solid-state NMR: A unified description using bimodal Floquet theory, *J. Phys. Chem.* 123 (2005) 064102.
- ³⁰A. Equbal, M. Leskes, N.C. Nielsen, P.K. Madhu, S. Vega, Relative merits of rCW(A) and XiX heteronuclear spin decoupling in solid-state magic-angle-spinning NMR spectroscopy: A bimodal Floquet analysis, *J. Magn. Reson.* 263 (2016) 55.
- ³¹F.J. Dyson, The radiation theories of Tomonaga, Schwinger, and Feynman, *Phys. Rev.* 75 (1949) 486.
- ³²J. H. Shirley, Solution of the Schrödinger equation with a Hamiltonian periodic in time, *Phys. Rev.* 138 (1965) B979.
- ³³G. J. Boender, S. Vega, H. J. M De Groot, A physical interpretation of the Floquet description of magic angle spinning nuclear magnetic resonance spectroscopy, *Mol. Phys.* 95 (1998) 921.
- ³⁴I. Scholz, P. Hodgkinson, B.H. Meier, M. Ernst, Understanding two-pulse phase-modulated decoupling in solid-state NMR, *J. Chem. Phys.* 130 (2009) 114510.
- ³⁵W. R. Hamilton. *Elements of Quaternions*. Chelsea, New York, 3rd edition (1969).
- ³⁶L. Emsley and G. Bodenhausen. Optimization of shaped selective pulses for nmr using a quaternion description of their overall propagators, *J. Magn. Reson.* 97 (1992) 135.
- ³⁷M. Leskes, P.K. Madhu, S. Vega, Floquet theory in solid-state nuclear magnetic resonance, *Progress in Nucl. Mag. Reson. Spectrosc.* 57 (2010) 345.
- ³⁸M. Leskes, R.S. Thakur, P.K. Madhu, N.D. Kurur, S. Vega, A Bimodal Floquet description of heteronuclear dipolar decoupling in solid state nuclear magnetic resonance, *J. Chem. Phys.* 127 (2007) 24501.

- ³⁹Y. Ernst, H. Geen, B.H. Meier, Amplitude-modulated decoupling in rotating solids: A bimodal Floquet approach, *Solid State Nucl. Magn. Reson.* 29 (2006) 2.
- ⁴⁰R. Ramachandran, M. S. Krishnan, Effective Hamiltonians in Floquet theory of magic angle spinning using van Vleck transformation, *J. Chem. Phys.* 114 (2001) 5967.
- ⁴¹M. K. Pandey, R. Ramachandran, Operator-based analytic theory of decoherence in NMR, *Mol. Phys.* 109 (2010) 1545.
- ⁴²M. K. Pandey, Z. Qadri, R. Ramachandran, Understanding cross-polarization (CP) NMR experiments through dipolar truncation, *J. Chem. Phys.* 138 (2013) 114108.
- ⁴³G. Metz, X.L. Wu, S.O. Smith, Ramped-amplitude cross polarization in magic angle spinning NMR, *J. Magn. Reson.* 110 (1994) 219.
- ⁴⁴M. Bak, J.T. Rasmussen, N.C. Nielsen, SIMPSON: A general simulation program for solid-state NMR spectroscopy, *J. Magn. Reson.* 147 (2000) 296.
- ⁴⁵Z. Tosnér, R. Andersen, B. Stevansson, M. Edén, N.C. Nielsen, T. Vosegaard, Computer-intensive simulation of solid-state NMR experiments using SIMPSON, *J. Magn. Reson.* 246 (2014) 79.
- ⁴⁶S. Smith, T. Levante, B. H. Meier, R. Ernst, Computer simulations in magnetic resonance: an object oriented programming approach, *J. Magn. Reson.* 106 (1994) 75.
- ⁴⁷M. Bak, R. Schultz, T. Vosegaard, N.C. Nielsen, Specification and visualization of anisotropic interaction tensors for numerical simulation of solid-state NMR experiments on polypeptide structures, *J. Magn. Reson.* 154 (2002) 28.
- ⁴⁸M. Bak, N.C. Nielsen, REPULSION, A novel approach to efficient powder averaging in solid-state NMR, *J. Magn. Reson.* 125 (1997) 132.

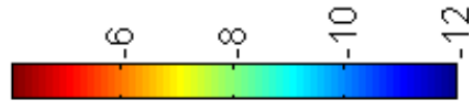
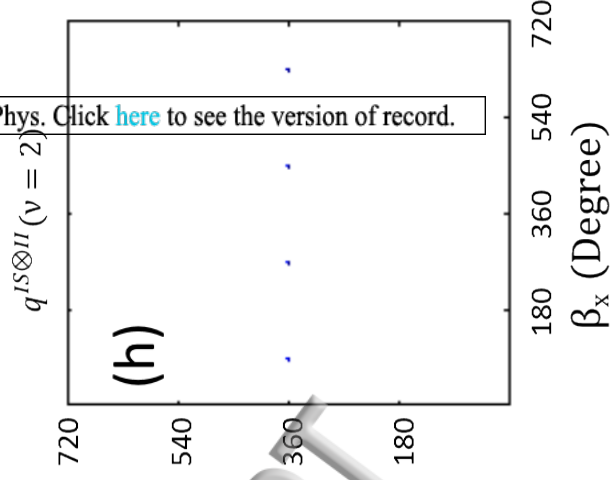
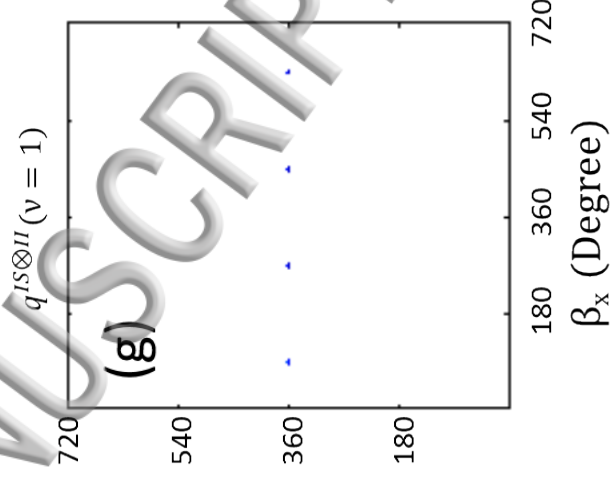
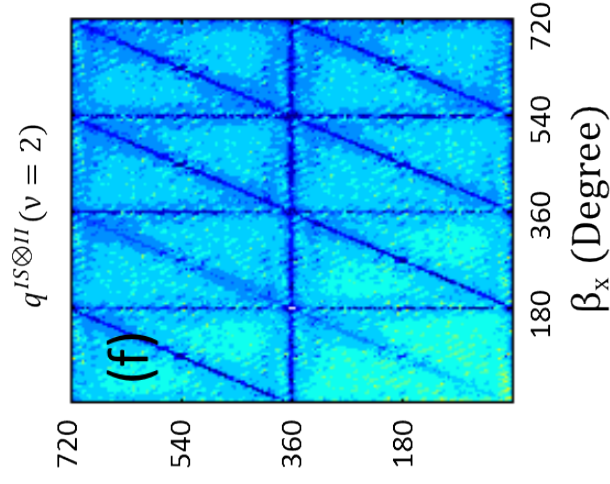
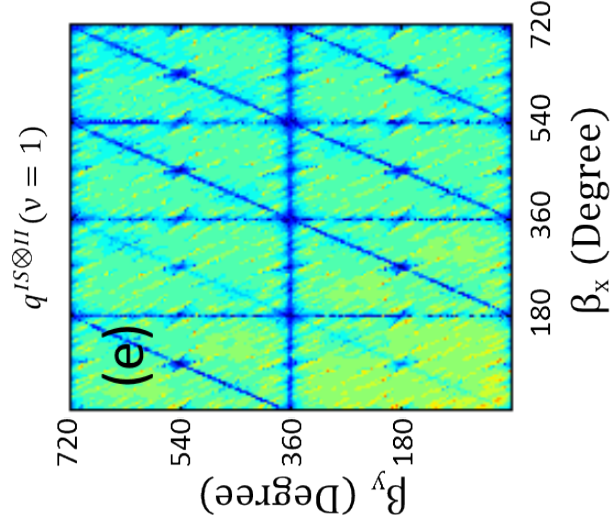




rCWA



rCWA_{ApA}



This manuscript was accepted by J. Chem. Phys. Click [here](#) to see the version of record.

ACCEPTED MANUSCRIPT

